Int. J. Electrochem. Sci., 12 **(2017)** 7911 – 7920, doi: 10.20964/2017.08.40

International Journal of ELECTROCHEMICAL SCIENCE
www.electrochemsci.org

A label-free Electrochemical Immunosensor for Anti-Mullerian Hormone Detection on Graphene-Au Nanocomposite

Lingling Li, Yongling Yu, Ping Chen and Weixia Liu[*]

The First Affiliated Hospital of Henan University of Traditional Chinese Medicine, Zhengzhou, 450000, China
[*]E-mail: liuweixia68@aliyun.com

Received: 23 April 2017 / *Accepted:* 2 June 2017 / *Published:* 12 July 2017

This study reported the construction of a graphene sensor based on poly(3,4-ethylenedioxythiophene)/Au nanoparticles, abbreviated as AuNPs/PEDOT/GR. The fabrication process consisted of two steps. First, the synthesis of PEDOT nanorods grown on graphene oxide nanosheets (PEDOT/GO) was conducted via liquid–liquid interfacial polymerization. Then, HAuCl4 was chemically reduced by NaBH4. The determination of anti-Mullerian hormone (AMH) was realized using a sensitive and facile AuNPs/PEDOT/GR-based immunosensor by measuring the electrochemical response variation before and after the immunoreaction.

Keywords: Anti-mullerian hormone; Poly(3,4-ethylenedioxythiophene); Electrochemical immunoassay; Graphene; Au nanoparticles

1. INTRODUCTION

Anti-Müllerian hormone, abbreviated AMH, is a protein that is encoded by the AMH gene in humans. This hormone inhibits the development of the Müllerian ducts in the male embryo [1, 2]. AMH expression has been considered exclusive to male Sertoli cells, although the expression of the AMH receptor could be observed in both male and female foetuses [3, 4]. Initiated by SOX9 in the Sertoli cells of males, AMH expression could lead to irreversible Müllerian duct regression. AMH expression appears to be closely regulated by FSH, DAX1, SF1 and GATA factors due to the significance of AMH expression for sex differentiation at a certain time during foetal development [5, 6]. It has been reported that mutations in either type II AMH receptor or the AMH gene could lead to the persistence of Müllerian derivatives in males that were originally approaching virilization. The ovarian granulosa cells of postpartum females could also be observed with AMH expression, which

functions as a molecular biomarker for the relative size of the ovarian reserve [7-9]. For humans, the prediction of menopause timing could be achieved by using the number of cells in the follicular reserve. For bovines, by predicting the number of antral follicles that developed to ovulation, females could be selected with AMH during multi-ovulatory embryo transfer programs [10-12].

AMH inhibits Müllerian duct development into Müllerian structures, such as the uterus in mammals. It has an ipsilateral effect. Specifically, the testis on one side inhibits the development of the Müllerian on this side [13, 14]. This effect appears within the first 8 weeks of human gestation. For the no gonads-produced hormone, there would be an automatic development of the Müllerian ducts and automatic death of the Wolffian ducts associated with the male reproductive organs. The assessable amount of AMH in the blood varies according to the sex and age [15-17]. AMH functions by interacting with specific receptors on target tissue cell surfaces. One of its most famous and specific effects, under the mediation of the AMH type II receptors, is the programmed cell death of the target tissue, such as foetal Müllerian ducts. In the reproductive years, AMH is expressed by granulosa cells of the ovary, and it restricts primary follicle formation via the FSH-induced inhibition of excessive follicular recruitment. Several researchers have claimed that it can be used to measure some specific aspects of ovarian function, such as premature ovarian failure, polycystic ovary syndrome and other disorders [18-20]. It is also of use in predicting an undesirable ovarian response during *in vitro* fertilization (IVF) without predicting the success rates of an already established pregnancy after IVF. Furthermore, the levels of AMH have been used to determine the residual egg reserve for a woman [21-23]. According to the aforementioned studies, AMH detection is of vital importance in the clinical setting.

Immunosensors can be categorized into two types, the labelled type and label-free type, according to the presence or absence of labels. Generally, a majority of the labelled type have to adopt certain materials as the second antibody's marker [24]. Nevertheless, several other chemicals and processes are essential for controlling the activity of the synthesized conjugates. A label-free immunosensor has the characteristics of facile fabrication, low cost, and desirable activity conservation for antigens and antibodies, and it has thus been appealing to many researchers. The feature of the electrode interface is remarkably crucial to the behaviour of an electrochemical immunosensor. In recent years, the synthesis of graphene or graphene derivatives, conducting polymers and other nanocomposites has become increasingly appealing because of their synergistic effects [25]. In terms of the conducting polymers, poly(3,4-ethylenedioxythiophene), also abbreviated as PEDOT, is electrochemically active, electrically conductive, environmentally stable, and transparent when doped, and it has been the most extensively studied [26]. Furthermore, PEDOT nanostructures with nanotubes and nanorods are capable of providing amplified sensitivity, and they possess a high surface area. Additionally, they have been considered remarkable sensing materials [27]. Ordinarily, a powerful, controlled template technique has been extensively used to fabricate nanostructures. Compared with carbon nanotube carbon fibres and fullerenes as well as other traditional carbon materials, the distinct graphene oxide (GO), an oxygenated derivative of graphene (GR) with carboxyl, carbonyl, hydroxyl and epoxy groups on the single atomic layer of carbon, is better [28]. GO has the potential to prepare nanocomposites as a remarkable template or filler due to its large surface area and desirable thermal, mechanical and structural features. Therefore, PEDOT/GO nanocomposites could be easily

synthesized through a facile liquid–liquid interfacial polymerization process because they could be simply synthesized and purified without needed a moving template [29]. As one of the electroactive noble materials, Au nanoparticles (AuNPs) are desirably stable, conductive, and biocompatible, they can be easily and rapidly synthesized, and they possess a narrow size distribution; therefore, they are extensively used in electrochemical immunosensor preparation [30]. Additionally, not only could more active sites be offered by AuNPs binding to antibodies, but they could accelerate the electron transfer process to amplify signals and achieve high sensitivity [31]. Before application in the electrochemical immunosensor preparation, AuNPs should be loaded onto nano-matrices to further increase the surface-to-volume ratio and enhance the conductivity.

This study proposed a novel electrochemical immunosensor modified by AuNPs/PEDOT/GR to detect AMH. The fabrication of this nanocomposite included two steps. A facile liquid–liquid interfacial polymerization was used to synthesise PEDOT/GO, which was followed by the chemical reduction of the mixture of $HAuCl_4$ and the as-prepared PEDOT/GO by $NaBH_4$ at ambient temperature. AuNPs and GR were generated under reduction from $HAuCl_4$ and GO, respectively. The significant enhancement in both the immobilizing level of antibody on the surface of the electrode and the electrical signal could be achieved because the as-prepared AuNPs/PEDOT/GR was appropriately biocompatible and had a remarkably large specific surface area and electron transfer capacity. The proposed immunosensor displayed a favourable response in AMH determination and has the potential for real specimen detection.

2. EXPERIMENTS

2.1. Chemicals

AMH and anti-AMH antibody were commercially available from Bosai Biotechnology co., Ltd. Graphene oxide (GO) was commercially available from Nanjing Xianfeng nano Co. 3,4-ethylenedioxythiophene (EDOT) and bovine serum albumin (BSA) were commercially available from Sigma-Aldrich. $HAuCl_4 \cdot 3H_2O$ was commercially available from Sinopharm Chem. Re. Co. Ltd. The diameter and the thickness of the GO were, respectively, ca. 1–5 nm and ca. 0.8–1.2 nm. Additionally, 0.1 M phosphate buffer solution (PBS; pH 7.0) was used as an electrolyte throughout the electrochemical tests. Double distilled water was used in all tests. All other reagents were of analytical grade and used without further purification.

2.2. Preparation of PEDOT/GO and AuNPs/PEDOT/GR nanocomposites

After the addition of $FeCl_3$ (1 mL, 1 M) into aqueous GO dispersion (1 mL, 0.5 mg/mL), the obtained mixture was sonicated for 10 min and slowly introduced into 2 mL of EDOT solution in $CHCl_3$ (25 mg/mL). Then, an interface was yielded between two layers. The as-prepared solution was heated at 50 °C under static conditions and left to react for 24 h. This was followed by the centrifugation of the upper layer mixture and several iterations of precipitate washing with distilled

water and ethanol. Then, the terminal precipitates were collected before use. The second step began with the dispersion of the as-prepared PEDOT/GO precipitates into deionized water under sonication. Before AuNPs were loaded, all glassware was soaked in a mixed solution of hydrochloric acid and nitric acid (3:1) for 60 min, followed by thorough washing with deionized water. Then, 8 mL of the aforementioned PEDOT/GO suspension was mixed with an aqueous solution of $HAuCl_4 \cdot 3H_2O$ (1 mL, 5 mM) under vigorous stirring. After 15 min, 0.1 M $NaBH_4$ aqueous solution was added, and the mixture was stirred for another 6 h at ambient temperature. Au ions and GO were both thoroughly reduced during reduction. Eventually, the terminal AuNPs/PEDOT/GR was collected, which was followed by washing, re-dispersion into water (1 mL) and storage at 4 °C before use.

2.3. Immunosensor fabrication

After mechanical polishing using chamois leather containing an alumina slurry (0.05 μm), the glassy carbon electrode (GCE) was cleaned using distilled water, absolute ethanol and double-distilled water (each for 5 min) under ultra-sonication. After transfer onto the GCE surface, the AuNPs/PEDOT/GR suspension (5 μL) was left drying in air. This was followed by the incubation of the as-prepared AuNPs/PEDOT/GR/GCE in 20 μg/mL anti-AMH antibody solution for the immobilization of antibody molecules onto the AuNPs surface (Ab/AuNPs/PEDOT/GR/GCE). After washing and the addition of BSA (5 μL, 1 wt%) (BSA/Ab/AuNPs/PEDOT/GR/GCE), the modified electrode was incubated in AMH with varied concentrations at ambient temperature for 50 min, and it was thoroughly washed to remove the unbound AMH molecules.

2.4. Electrochemical determination

Differential pulse voltammetry (DPV) was recorded at a potential from ―0.2 to 0.6 V (vs. SCE), with a pulse period of 0.2 s and amplitude of 50 mV. Electrochemical impedance spectroscopy (EIS) was recorded within a frequency range from 0.1 Hz to 100 kHz and with an amplitude of 5 mV. X-ray diffraction (XRD) patterns were recorded on a Rigaku powder diffractometer equipped with Cu_{Ka} 1 radiation (l ¼ 1.5406 °A). A Raman spectrum (Bruker Raman RM2000) was used to analyse the samples with a 785-nm laser. Infrared spectra were recorded using a Bruker Vertex 70 Fourier spectrometer with samples in KBr pellets.

3. RESULTS AND DISCUSSION

Fig. 1A shows the FT-IR spectra of PEDOT/GO (a) and AuNPs/PEDOT/GR (b). The former spectrum showed a characteristic peak at 1732 cm^{-1}, corresponding to the C=O stretching, indicating the presence of oxygen functionalities on the surface of GO. In the latter spectrum, bands ascribed to the OH stretching and absorbed water (3382 cm^{-1}), C=C (1634 cm^{-1}), C–C (1403 cm^{-1}), and C–O–C (1097 cm^{-1}) could also be observed. In addition, other adsorption peaks can be observed at 824 and 683 cm^{-1}, which are attributed to the vibration modes of C–S–C bond of thiophene ring. There was a remarkable decrease in the absorption peaks at 1732 and 1091 cm^{-1} in the FTIR spectra of

AuNPs/PEDOT/GR compared with PEDOT/GO, which indicated that the GO was effectively transformed into GR in the process of synthesis [32].

Raman spectroscopy was further used to evaluate the nature and relative quantities of carbonaceous materials that formed on the particle surfaces in the as-prepared composites [33]. PEDOT/GO and AuNPs/PEDOT/GR composites were characterized via Raman spectra in Fig. 2B. The characteristic peaks observed at 441, 573 and 1102 cm^{-1} for both were ascribed to the deformation of the C–O–C bond. Vibrational modes at 852 and 985 cm^{-1} were attributed to the deformation of O–C–C and oxyethylene ring. The peaks observed at 1254 and 1364 cm^{-1} were assigned to the thiophene C–C inter-ring stretching. The peaks at 1423 and 1505 cm^{-1} were ascribed to symmetric and antisymmetric C=C stretching, respectively. In the spectrum of the latter composite, a shift of a band of PEDOT/GO at 1562 cm^{-1} to 1551 cm^{-1} could be observed, which was possibly from the reduction of GO in this composite into GR.

Fig. 1C displayed the XRD profiles characterizing the structure of the PEDOT/GO and AuNPs/PEDOT/GR nanocomposites. In the profile of the former nanocomposite, the clear peak at ca. 11.8° was absent from the latter nanocomposite, thus confirming the removal of a majority of oxygen functional groups and the successful reduction of GO into GR. In addition, a broad diffraction peak at $2\theta = 26.9°$ could be observed for the PEDOT/GO, which was possibly assigned to the (020) reflection or intermolecular spacing of polymer backbone [34, 35]. Moreover, the diffraction characteristics observed at 2θ, 38.33°, 44.55°, 64.77°, 77.88° and 81.96°, which correspond to the (111), (200), (220), (311) and (222) planes of the standard cubic phase of Au, respectively, could be confirmed by the results of XRD measurement for AuNPs/PEDOT/GR.

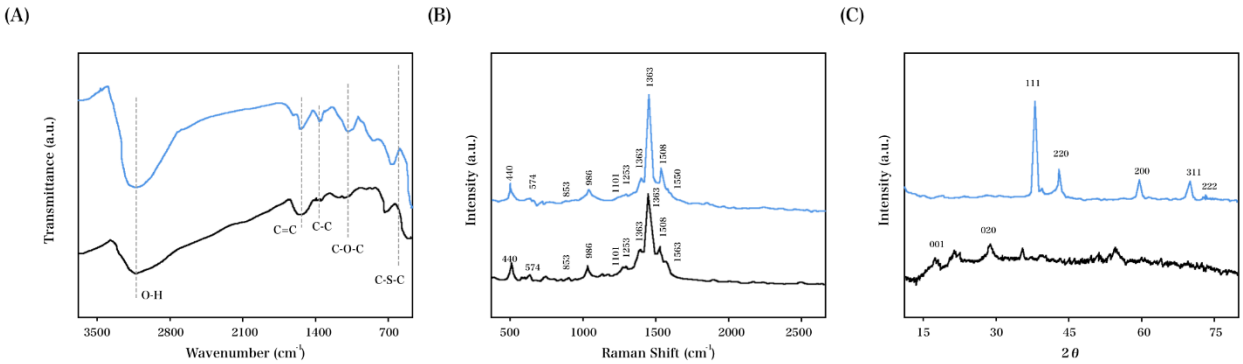

Figure 1. (A) FT-IR, (B) Raman spectroscopy and (C) XRD profiles of PEDOT/GO and AuNPs/PEDOT/GR.

Electrochemical impedance spectroscopy (EIS) is an effective tool for monitoring the interface properties of surface modified electrodes. EIS measurement was employed for the stepwise preparation of the proposed immunosensor. The electron transfer resistance (R_{et}) was represented by the semicircle diameter in a Nyquist plot of Fig. 2. The R_{et} was calculated by fitting the data to an equivalent electrical circuit. A desirable impedimetric performance of the original GCE was displayed through the

corresponding Nyquist spectrum. Other modified electrodes exhibited a drop of the semicircle diameter, ascribed to the facilitation of the electron transportation of the redox moieties onto the electrode by the modification layer. After anti-AMH was immobilized onto the AuNPs/PEDOT/GR, there was an increase in R_{et}, due to the insulation property of anti-AMH. After BSA was added, R_{et} continued to increase because any residual free spaces were blocked on the electrode. The further R_{et} increase caused by the addition of AMH indicated that an immunocomplex was formed, which was likely because the anti-AMH was successfully immobilized on the surface and formed an additional barrier that blocked the electron exchange between the redox probe and electrode. Triplicates of the EIS assays were performed. Through data fitting, the standard deviations were calculated within 6%.

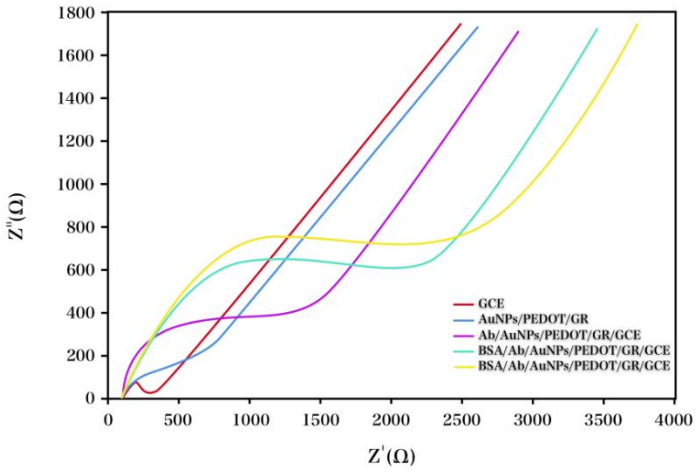

Figure 2. Nyquist plots of the stepwise modification of the nanocomposite cryogel electrode: bare GCE, AuNPs/PEDOT/GR, Ab/AuNPs/PEDOT/GR/GCE, BSA/Ab/AuNPs/PEDOT/GR/GCE and BSA/Ab/AuNPs/PEDOT/GR/GCE.

The incubation time, incubation temperature and buffer pH value all affect the behaviour of the proposed immunosensor. The test solution at pH values ranging from 5.5 to 8.0 was used to study the effect of pH on the performance of the proposed immunosensor in detecting AMH (1 ng/mL). With the increase in the pH from 5.5 to 7.0, the current response showed an increase and reached a plateau, and it then decreased with a further pH increase to 8.0. Therefore, pH 7.0 was obtained as the optimal pH value for all tests to ensure a desirable sensitivity. The incubation time is also a vital factor in the immunosensor fabrication. The proposed immunosensor was incubated in AMH with a constant concentration for varied time periods (Fig. 3B). There was a rapid increase in the ΔI (the change of the current response) in the first 55 min, which subsequently dropped. Hence, the optimized incubation time was 55 min. The temperature in a range of 10 - 50 °C was applied to study its effect on the current responses. The effect of temperature on the current responses was also studied. The maximal response was obtained at 30 °C (Fig. 3C). Nevertheless, AMH and anti-AMH would be irreversibly denaturated with a further temperature increase to 35 °C. It has been well acknowledged that the modifier would be damaged and that the immunosensor's lifetime would be affected when used at a high temperature for a long time. Hence, the optimized temperature for immunoreactions was 30 °C.

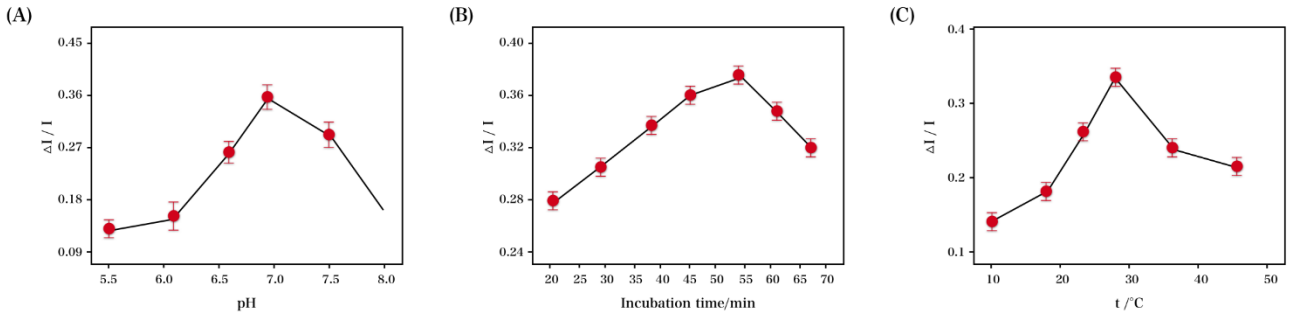

Figure 3. Effect of the (A) pH of PBS, (B) incubation time and (C) incubation temperature on the current responses of the proposed immunosensor.

AMH concentrations were detected using a differential pulse voltammetry (DPV) assay in PBS (pH 7.0) containing $Fe(CN)_6^{3-/4-}$ (5.0 mM) solution to evaluate the dynamic working range and sensitivity of the proposed immunosensor. With the increase in the concentration of AMH, there was a decrease in the current signal of DPV (Fig. 4). One reason could be that the insulation of the AMH protein layer acting as a nonconductor obstructed the electron transfer between the electrolyte and electrode surface [36]. That is, as the concentration of AMH increased, there was a decrease in the DPV response of the proposed immunosensor, which was linearly related to the logarithm of the AMH concentration in a range of 0.0004 - 40 ng/mL. Herein, the relative standard deviations (RSD) and limit of detection (LOD) were calculated as below 3.6% and 0.21 pg/mL (S/N=3), respectively. The sensitivity of the BSA/Ab/AuNPs/PEDOT/GR/GCE was compared to that of other reported, modified electrodes, and the results are presented in Table 1.

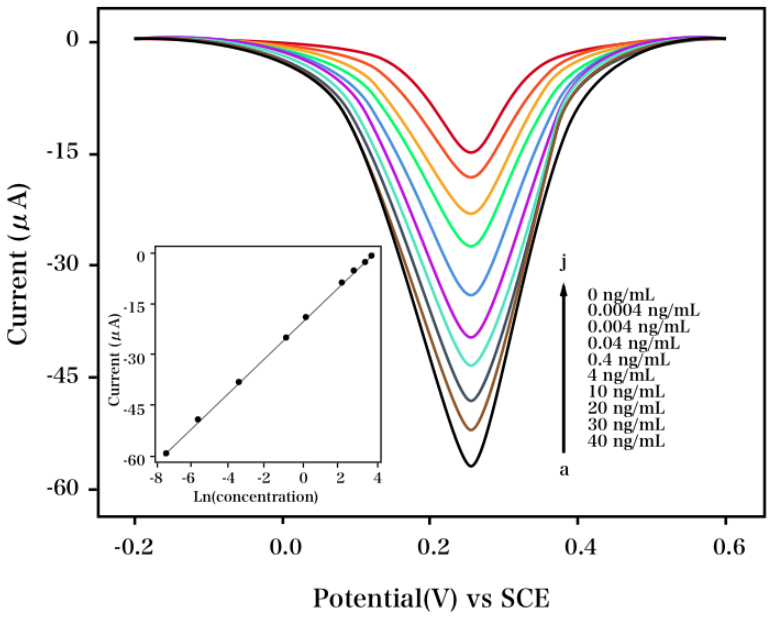

Figure 4. DPV of the proposed immunosensor after incubation in AMH at varied concentrations (0, 0.0004, 0.004, 0.04, 0.4, 4, 10, 20, 30 and 40 ng/mL).

Table 1. Comparison of the present BSA/Ab/AuNPs/PEDOT/GR/GCE with other AMH determination methods.

Method	Linear detection range	Detection limit	Reference
Enzyme-linked immunosorbent assay	0.04 to 20 ng/mL	4 pg/mL	[1]
Enzyme-linked immunosorbent assay	—	7 pg/mL	[37]
Enzyme-linked immunosorbent assay	—	0.05 ng/mL	[38]
BSA/Ab/AuNPs/PEDOT/GR/GCE	0.0004to 40 ng/mL	0.21 pg/mL	This work

To further validate the developed immunoassay, five rabbit tumour model samples were analysed using the conventional immunohistochemical staining method and proposed immunosensor. The results are shown in Table 2. The relevant faults were less than 3.17%, which indicated that the results from the two approaches agreed with each other.

Table 2. Real sample test use proposed BSA/Ab/AuNPs/PEDOT/GR/GCE and immunohistochemical staining method.

Sample	Immunosensor (ng/mL)	Immunohistochemical staining (ng/mL)	RSD (%)
1	4.51	4.49	3.17
2	5.21	5.77	2.30
3	10.29	10.11	1.21
4	12.21	12.09	1.46
5	15.30	15.28	1.22

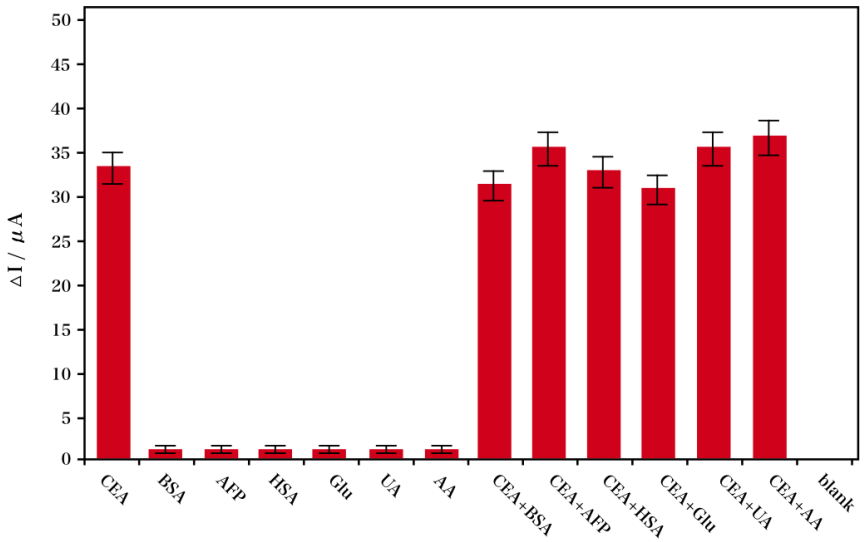

Figure 5. Responses of the proposed immunosensor for AMH detection and different potential interferences.

Fig. 5 indicates that the current response for AMH (0.5 ng/mL) is 34 μA and that other potential interference molecules display much lower current variations. The current variations were very much lower than the LOD signal, and they were nearly the same as that of the buffer (blank) response. With the mixture of each interference compound with the AMH, the interference-induced change was below 4% without an obvious difference ($P > 0.05$) with statistical test. It can be concluded that the proposed immunosensor is appropriately selective for AMH detection.

4. CONCLUSIONS

This work explored the determination of AMH using a novel electrochemical immunosensor based on a AuNPs/PEDOT/GR nanocomposite. The synthesized nanocomposite is appropriately biocompatible and conductive, and it possesses a large specific surface area. These favourable properties contribute to the remarkable sensitivity enhancement of the proposed sensor. This immunosensor displayed a wide linear range and low LOD under optimal circumstances.

ACKNOWLEDGEMENTS
This Work Supported by Foundation of Henan Special Subject of Scientific Research of Traditional Chinese Medicine (NO.2016ZY2007)

References

1. C. Clark, C. Laskin and K. Cadesky, *Human Reproduction*, 29 (2014) 184.
2. C. Harden, P. Pennell, J. French, A. Davis, C. Lau, N. Llewellyn, B. Kaufman, E. Bagiella and A. Kirshenbaum, *Epilepsy Research*, 127 (2016) 66.
3. A. Liang, A. Salzano, M. D'Esposito, A. Comin, M. Montillo, L. Yang, G. Campanile and B. Gasparrini, *Theriogenology*, 86 (2016) 963.
4. M. Garin, S. Butts, D. Sarwer, K. Allison, S. Senapati and A. Dokras, *Endocrine*, (2016) 1.
5. E. Carmina, F. Fruzzetti and R.A. Lobo, *American Journal of Obstetrics and Gynecology*, 214 (2016) 714.
6. A. Pacchiarotti, P. Frati, G. Milazzo, A. Catalano, V. Gentile and M. Moscarini, *European Journal of Obstetrics & Gynecology and Reproductive Biology*, 172 (2014) 62.
7. E. Somigliana, M. Marchese, M. Frattaruolo, N. Berlanda, L. Fedele and P. Vercellini, *European Journal of Obstetrics & Gynecology and Reproductive Biology*, 180 (2014) 142.
8. P. Bhide, A. Gudi, A. Shah and R. Homburg, *BJOG: An International Journal of Obstetrics & Gynaecology*, 122 (2015) 1625.
9. B. Deubzer, K. Weber, B. Lawrenz, R. Schweizer and G. Binder, *The Journal of Clinical Endocrinology & Metabolism*, 99 (2014) E1045.
10. H. Li, V. Lee, E.Y.L. Lau, W. Yeung, P. Ho and E Ng, *PloS one*, 8 (2013) e61095.
11. S. Elchuri, B. Patterson, M. Brown, I. Buchanan, A. Mertens and L. Meacham, *Journal of Pediatric Endocrinology and Metabolism*, 28 (2015) 189.
12. L. Nappi, S. Angioni, F. Sorrentino, G. Cinnella, M. Lombardi and P. Greco, *Gynecological Endocrinology*, 32 (2016) 34.
13. F. Chiofalo, C. Ciuoli, C. Formichi, F. Selmi, R. Forleo, O. Neri, G. Vuolo, P. Paffetti and F. Pacini,

Obesity Surgery, (2016) 1.
14. H. Schock, E. Lundin, M. Vääräsmäki, K. Grankvist, A. Fry, J. Dorgan, E. Pukkala, M. Lehtinen, H. Surcel and A. Lukanova, *Cancer Causes & Control*, 25 (2014) 583.
15. C. Rongieres, C. Colella and P. Lehert, *Journal of Assisted Reproduction and Genetics*, 32 (2015) 37.
16. M. Dayal, S. Sagar, A. Chaurasia and U. Singh, *The Journal of Obstetrics and Gynecology of India*, 64 (2014) 130.
17. J. Hou, H. Cook-Andersen, H. Su, R. Shayya, K. Maas, C. Burt-Solorzano, A. Kumar and R. Chang, *Journal of Pediatric Endocrinology and Metabolism*, 29 (2016) 835.
18. A. Tokmak, D. Kokanali, H. Timur, M. Kuntay Kokanali and N. Yilmaz, *Gynecological Endocrinology*, 32 (2016) 926.
19. A. Stojsin-Carter, K. Mahboubi, N.N. Costa, D.J. Gillis, T. Carter, M. Neal, M. Miranda, O. Ohashi, L. Favetta and W. King, *Animal Reproduction Science*, 167 (2016) 51.
20. J. Baldrighi, M. Sá Filho, E. Batista, R. Lopes, J. Visintin, P. Baruselli and M. Assumpção, *Reproduction in Domestic Animals*, 49 (2014) 1015.
21. A. Sopher, G. Grigoriev, D. Laura, T. Cameo, J. Lerner, R. Chang, D. McMahon and S. Oberfield, *Journal of Pediatric Endocrinology and Metabolism*, 27 (2014) 1175.
22. M. Vega, D. Barad, Y. Yu, S.K. Darmon, A. Weghofer, V. Kushnir and N. Gleicher, *American Journal of Reproductive Immunology*, 76 (2016) 333.
23. B. Guerreiro, E. Batista, L. Vieira, M. Sá Filho, C. Rodrigues, A. Netto, C. Silveira, B. Bayeux, E. Dias and F. Monteiro, *Domestic Animal Endocrinology*, 49 (2014) 96.
24. G. Sun, J. Lu, S. Ge, X. Song, J. Yu, M. Yan and J. Huang, *Anal. Chim. Acta.*, 775 (2013) 85.
25. W. Lei, W. Si, Y. Xu, Z. Gu and Q. Hao, *Microchim. Acta.*, 181 (2014) 707.
26. L. Groenendaal, F. Jonas, D. Freitag, H. Pielartzik and J.R. Reynolds, *Adv. Mater.*, 12 (2000) 481.
27. F. Jiang, R. Yue, Y. Du, J. Xu and P. Yang, *Biosensors and Bioelectronics*, 44 (2013) 127.
28. Y. Gao, L. Wu, K. Zhang, J. Xu, L. Lu, X Zhu and Y. Wu, *Chinese Chemical Letters*, 26 (2015) 613.
29. Q. Hao, H. Wang, X. Yang, L. Lu and X. Wang, *Nano Research*, 4 (2011) 323.
30. E. Afoakwa, E. Ofosu-Ansah, J. Takrama, A. Budu and H. Mensah-Brown, *International Food Research Journal*, 21 (2014)
31. L. Zhu, L. Xu, N. Jia, B. Huang, L. Tan, S. Yang and S. Yao, *Talanta*, 116 (2013) 809.
32. Y. Gao, J. Xu, L. Lu, X. Zhu, W. Wang, T. Yang, K. Zhang and Y. Yu, *RSC Advances*, 5 (2015) 86910.
33. S. Yoon and K. Kim, *Electrochimica Acta*, 106 (2013) 135.
34. N. Hui, S. Wang, H. Xie, S. Xu, S. Niu and X. Luo, *Sensors and Actuators B: Chemical*, 221 (2015) 606.
35. K. Huang, L. Wang, Y. Liu, T. Gan, Y. Liu, L. Wang and Y. Fan, *Electrochimica Acta*, 107 (2013) 379.
36. L. Li, C. Ma, Q. Kong, W. Li, Y. Zhang, S. Ge, M. Yan and J. Yu, *Journal of Materials Chemistry B*, 2 (2014) 6669.
37. M. Kevenaar, M. Meerasahib, P. Kramer, B. van de Lang-Born, F. de Jong, N. Groome, A. Themmen and J. Visser, *Endocrinology*, 147 (2006) 3228.
38. W. Long, V. Ranchin, P. Pautier, C. Belville, P. Denizot, H. Cailla, C. Lhommé, J. Picard, J. Bidart and R. Rey, *The Journal of Clinical Endocrinology & Metabolism*, 85 (2000) 540.